MSEC2019-2926

MULTIPHASE FLOW DISTRIBUTION IN MQL DRILLING USING OPTICAL INTENSITY DISTRIBUTION BASED APPROACH

Jay K. Raval
Mechanical Engineering
Texas A&M University
College Station, TX 77843, USA

Wayne N. P. Hung
Engineering Technology
Texas A&M University
College Station, TX 77843, USA

Bruce L. Tai
Mechanical Engineering
Texas A&M University
College Station, TX 77843, USA

ABSTRACT

Oil flow distribution in Minimum Quantity Lubrication (MQL) plays an important role in the efficiency of machining processes, but it remains challenging to measure experimentally. This paper presents a new method to measure the oil flow distribution in through-channel drill bits based on the reflected light intensity. Measurements were conducted from multiple angles in order to map the flow distribution across the channel cross-sectional area. The method is applied to drill bits of a circular cross-section channel and two helix angles, 0° and 30°. The results show that, for the 0° helix angle channel, the oil concentrates near the periphery of the channel, while for 30° helix angle channel, the oil concentrates towards the center of the drill point. Furthermore, Computational Fluid Dynamics (CFD) simulation was conducted to compare with the measurement results, and it was observed that the oil distribution is correlated to the velocity field. Oil flow concentration is high in low velocity regions. Though preliminary, this study has concluded that the velocity field generated using single-phase CFD is a critical indicator for oil distribution in an MOL flow.

INTRODUCTION

Machining processes involve plastic deformation of the workpiece and removal in the form of chips. This shearing plastic deformation along with the friction between the tool and the workpiece generates a huge amount of thermal energy, which degrades the tool and its coating, and is an important cause of tool wear and tool failure [1, 2]. Hence, cutting fluids have been a common approach to deal with heat generation in machining. However, some cutting fluids may have a harmful effect on the worker's health, and increase social and economic

problems [3, 4]. These drawbacks can be abridged by employing Minimum Quantity Lubrication (MQL).

MQL, also known as near dry machining, uses a tiny quantity of lubricant in the form of a mist to aid machining process. The mist is atomized using pressurized air and delivered through either a nozzle directed towards the cutting zone or internal channels in the tool. In MQL drilling, the later system has proved to be more efficient because of its capability to deliver the mist directly to the cutting zone [5]. Also, unlike traditional flood cooling, which leaves the parts wet, the parts produced with MQL machining are almost dry and ready for the next process; this reduces the auxiliary time for the production and improves the efficiency of the whole plant [5]. Studies show that MQL provides better surface finish, tolerances, and a longer tool life when compared to flood cooling [6-10]. Considering all these advantages, MQL seems superior to the traditional flood cooling. Nevertheless, because of the sensitivity of the MQL process, a small deviation in flow condition can degrade the machining quality [11]. The heat flux generated at the cutting edge is not constant[12], more heat is generated at the chisel edge than at the periphery of the tool. If low quantities of lubricant is being used like in MQL, it is important to efficiently deliver the lubricant to the required location. Furthermore, a lot of research has been done on the effects of multiple parameters on their machining effectiveness [13-19] as well as on characterization of the mist flow in terms of the droplet size or velocity field [20-23]. However, only few studies have explored the flow structure (i.e., oil mist distribution in a flow), which eventually affects oil coverage on the cutting edges.

MQL is a two-phase flow. The characterization of flow can be complex as compared to a single-phase flow. Several methods are available for the analysis of two-phase flow, which can be broadly classified into invasive methods and noninvasive methods. Invasive methods usually measure the flow directly, such as using probes, but they can change the flow field, in particular for the small diameter of coolant delivery channels in MQL tools (often in the scale of 1 mm). Noninvasive techniques, on the other hand, do not interfere with the flow and hence provide more accurate flow results, but this advantage comes at the expense of computational effort required by the correlation algorithms. Common noninvasive experimental methods for the measurement of multiphase flow include Magnetic Resonance Imaging (MRI), Neutron and X-ray radiography, Phase Doppler Anemometry (PDA), and Particle Image Velocimetry (PIV)[24]. However, MRI cannot be used because MQL fluid does not respond to the magnetic field charge. Both PDA and PIV use high-speed imaging along with projecting bright laser sheets to track the particles thus, they cannot capture the non-planar flow structure. Furthermore, PIV can only generate the velocity field but not the phase distribution. The high working pressure (5-8 bars) and small channels in MQL produce a high flow velocity in the order of 100 m/s for droplet sizes less than 10 µm [25, 26]. Thus, planar particle tracking methods are not possible in the application of multiphase flow in internal cooling channels of a drill bit.

Henceforth, a new method is proposed, aimed to qualitatively compare the oil distribution across the channel using high speed imaging and intensity analysis of the image. In this study, the identified oil distribution and single-phase computational fluid dynamics simulation were compared to observe the correlation between the air flow and mist flow distribution.

To structure this paper, the experimental setup, methods, image acquisition and processing methods are explained in Section 2. Section 3 explains the results obtained after experiments for the multiple cases and is followed by Section 4 which shows the setup process for the numerical solution along with the comparison of the numerical and experimental results. Finally, Section 5 discusses the physics behind the phenomena and Section 6 draws the conclusions.

EXPERIMENTAL CONFIGURATION AND PROCEDURE

Experimental Setup

The focus of the study was on finding the oil distribution in internal channels of a drill bit employing MQL. A lab-scale setup was developed to emulate the actual MQL delivery process. The experimental setup as shown in Fig.1 consists of a dual channel MQL system (CoolubricatorTM, UNIST Inc., Grand Rapids, MI) which transfers the pressurized air and lubricant in separate concentric channels and atomizes the lubricant near the tool entry for more uniform mist at the exit. An MQL fluid, UNIST Coolube 2210, was used as the lubricant, which had an intermediate surface tension and viscosity among commonly used products [26]. The UNIST MQL system allowed flow rate control from 5 mL/hour to 50 mL/hour. The testing flow rate was fixed at 40 mL/hour in this

study to emulate the production setting. The MQL system was connected to a spindle shaft and a drill bit by a rotary union to allow rotary motion of the shaft without rotating the fluid tubes used to deliver MQL fluid. Finally, a high speed camera (Phantom Miro lab310) with a capacity of acquiring 3200 frames/sec (fps) greyscale images at 1280×800 resolution was used to capture the mist flow structure.

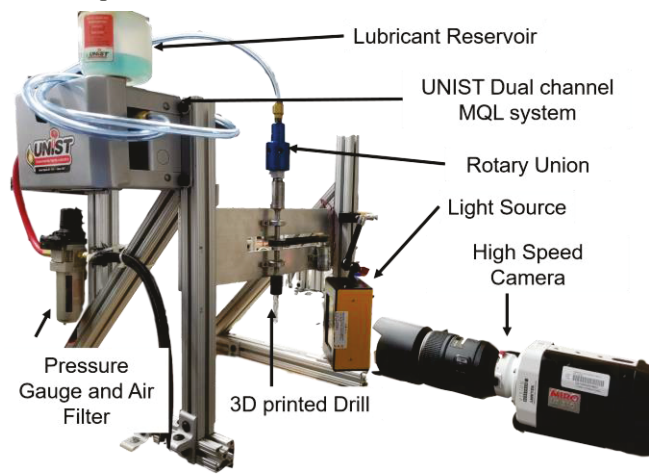


FIG. 1: EXPERIMENTAL SETUP FOR SIMULATING MQL FLOW IN INTERNAL CHANNEL DRILL BITS

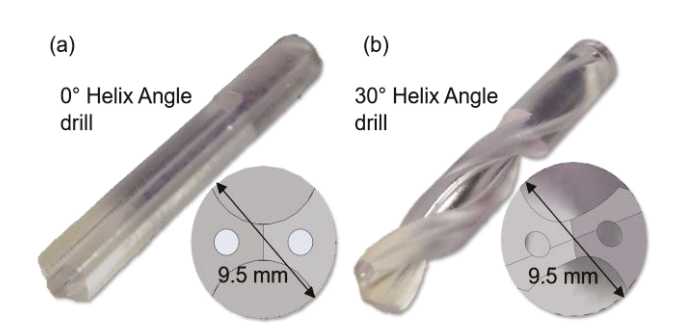


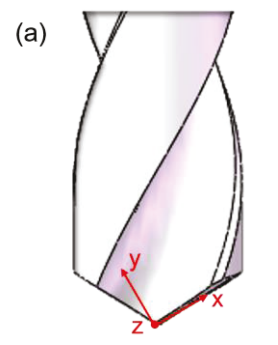
FIG. 2: DESIGNED DRILL BITS WITH TWO HELIX ANGLES

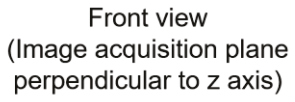
3D printing technology was used to design and fabricate drill bit with different channels as these drills were not going to be used for actual cutting. Moreover, customizing carbide drill bits can be time-consuming, costly and inefficient. Figure 2 shows two 3D printed drill bits with 0° and 30° helix angles, respectively, with an identical channel hole geometry (circle) of size 1.6 mm in diameter. These drill bits were made using a Stereolithography (SLA) 3D printer (Form 2, Somerville, MA). SLA produces a higher resolution (100 µm or less) and finer surface finish among available technologies, which allowed to precisely control the geometry of the tools and coolant channels. The surface-droplet interaction of the used photopolymer was confirmed by the contact angle of the lubricant oil. The measured angle ranged from 15° to 18°, which was similar to that on WC (commonly used cutting tool

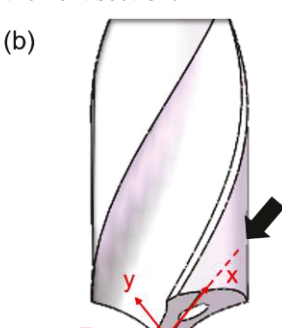
material) [16, 26]. The effect of surface roughness was not considered.

The current study was limited to a stationary condition because the rotation of the drill bit, except at ultra-high speed, has limited effect on the flow distribution due to the substantial velocity difference between the tangential direction (due to rotation) and the axial direction (due to pressure difference). This was supported by Johns et al. who used CFD to simulate the flow of coolant in internal channels of the drill and found out that the rotation of the drill does not produce any considerable effect of the velocity contours at exit [19]. This was verified by the MQL flow images captured by Kao et al. [27, 28].

In this study, flow images were captured at two different angles for a better understanding of the oil distribution in three dimensions. For experimentation, the camera was set and focused facing towards the drill bit as shown in Fig. 3(a). The MQL system was then turned on to initiate the flow for image acquisition. Once done, the drill bit was turned 90°, the camera was tilted to align with the cutting edge of the tool, and the same image acquisition procedure was repeated, as shown in Fig. 3(b). These two viewing angles are named front and side view, respectively. The geometry of the drill, as seen in Fig. 3(b), has dual clearance angles, these angles reduce the cutting forces acting on the tool. However, the difference between the two angles is too small and can be considered as a single angle for this study. Moreover, when looked from the side view, the flow from both the channels gets superimposed thus, to avoid this, other channel of the drill was closed for side view experiments so that there was no flow from the other channel. This resolved the problem of superposition of flow from two channels. Since the camera setup remains the same, all front and side view images have consistent irradiance. The image processing method is detailed in the next section.







Side view (Image acquisition plane perpendicular to x axis)

FIG. 3: VIEWING ANGLES OF DRILL FOR EXPERIMENTATION PURPOSE. (a) VIEWING ANGLE FOR FRONT VIEW (b) VIEWING ANGLE FOR SIDE VIEW Image Processing

In a multiphase flow where one of the media is transparent and the other is either translucent or opaque, optical imaging would only capture the non-transparent phase. This is advantageous when analyzing the distribution of the non-transparent phase in a continuous flow, such as solid particles in air flow. However, in the case of liquid droplets in a gas flow as in MQL, the light-droplet interaction is more complicated because of both light reflection and penetration, which conspire to make the identification of the droplet phase more difficult. This challenge can be mitigated by using a strong light source to increase the contrast and decrease any possible attenuation. Also, due to the transparency of the droplets, the image would appear in different intensities in grayscale when droplets overlay on each other. This characteristic can be used to determine the droplet concentration within a control volume.

Since the light is reflected from the whole 3D control volume, the image captured is a 2D projection of the 3D flow as shown in Fig. 4. Moreover, the aperture of the lens was kept f/2.8 mm so deeper depth of field can be obtained. For this reason, the image represents the superposition of droplets at multiple depths. Assuming no light attenuation, the light intensity at a pixel can be considered proportional to the total amount of the oil droplets along the depth of that pixel position. Hence, the brightness of the pixel can be used to represent the mass flow rate of oil droplets within that pixel location. Similarly, the intensity distribution along a reference line, as shown in Fig. 4 would represent the distribution of mass flow rate through a plane passing through the reference line and perpendicular to the viewing angle.

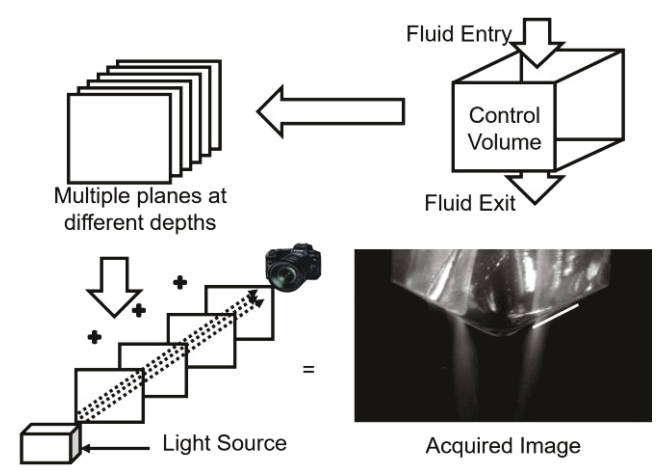


FIG. 4: SAMPLE IMAGE OF 2D PROJECTION OF 3D FLOW

Depending on the observation plane being normal to the drill axis (line 1 in Fig. 5) or parallel to the exit area of the channel (line 2 in Fig. 5), the reference line may represent either a circle or an ellipse, as shown in Fig. 5. Since the flow expands right after coming out of the nozzle, the measurement should be taken as close to the exit as possible. Thus, the elliptical observation plane was used for the flow profile analysis. In the case of a homogeneous dispersed mist flow as shown in Fig. 6 the projected intensity on the reference line (e.g., I_2) should be proportional to the corresponding depth of the ellipse (e.g., I_1).

As a result, despite homogeneous flow distribution, for both of these two angles, one can see a higher intensity at the center of the cross-section and lower intensity toward the two ends because of superposition of droplets.

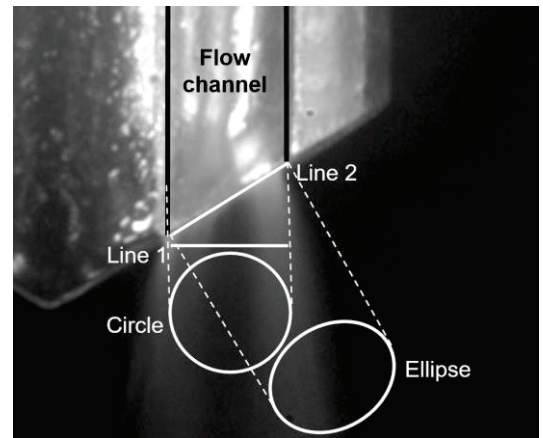


FIG. 5: CHANGE IN CROSS-SECTION GEOMETRY
BASED UPON THE VIEWING ANGLE

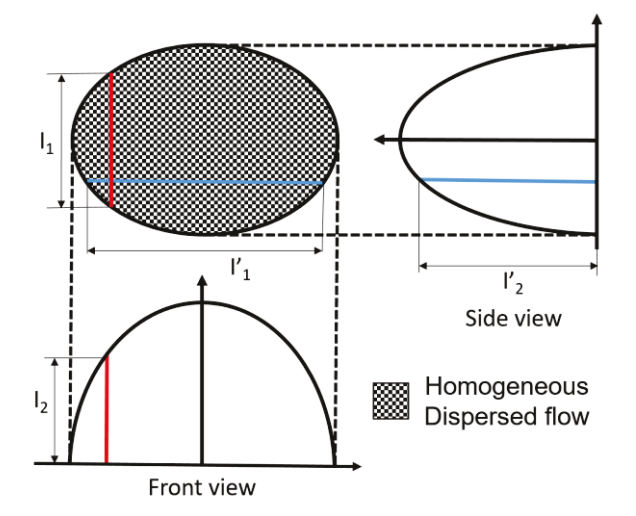


FIG. 6: BASELINE PROFILE GENERATION APPROACH USED FOR HOMOGENEOUS DISPERSED FLOW

Irradiance (i.e., the light coming from the light source) also affects the intensity profile generated. Thus, the dependence of irradiance from the profile must be removed by properly scaling and shifting the data, namely scaling. Figs. 7(a)-(c) show the images obtained for different irradiance levels of light. The raw intensity profiles along the reference line, are plotted in Fig. 7(d). As seen, the profiles have different intensity levels, and the starting and end points do not line up with the horizontal axis. The misalignment happens because of the ambient light or the light reflected from other objects in the room, hereafter termed as noise. To remove the noise, the profiles are shifted by subtracting the average background noise calculated from randomly selected 10 pixels in the dark zone. This step can align the starting and end points to the horizontal axis with very small errors remaining. The profiles are then scaled by the

maximum value of the pixel intensity in a profile. The scaled profiles are shown in Fig. 7(e). All the scaled profiles have a similar trend, which indicates that the scaling can remove the irradiance dependency of the data when comparing different cases.

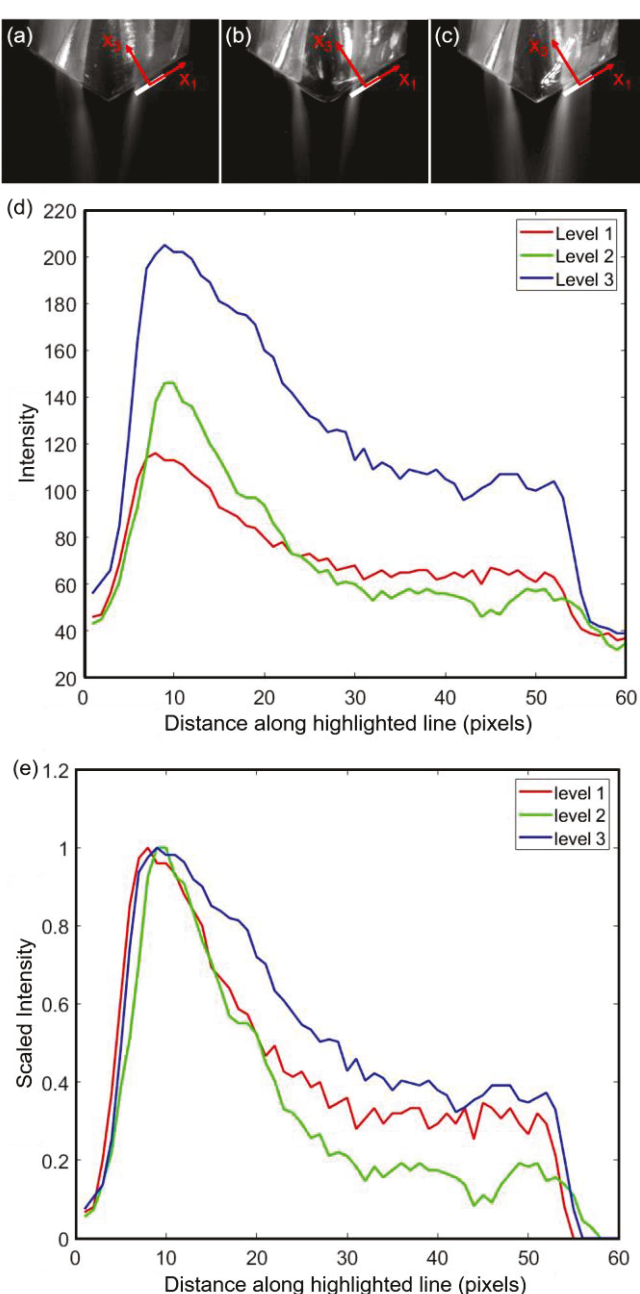


FIG 7: (a), (b), (c) SAMPLE IMAGES AT DIFFERENT IRRADIANCE INTENSITY LEVELS (WHITE LINE REPRESENTS THE LINE ACROSS WHICH INTENSITY IS PLOTTED) (d) INTENSITY PROFILE ALONG THE WHITE LINE (e) SCALED INTENSITY PROFILE ALONG WHITE LINE.

In order to clearly see how oil distributes in three dimensions from a 2D projected plot, the 2D profile of the

homogeneous dispersed flow (Fig. 6) can be used as the baseline. The baseline profile must be scaled so that the total intensity value (the area under the curve) is equal to that of the measured case (e.g., Fig. 7(e)). Then, the difference between the scaled measured and scaled baseline gives the Normalized profile. The normalized profile would indicate, high and low oil concentration areas with the averaged intensity being zero. A positive value in the normalized profile means higher droplet concentration as compared to the homogeneous dispersed flow conditions and a negative value means lower droplet concentration. The results are shown in the following section.

EXPERIMENTAL RESULTS

Figure 8 shows the images captured for a circular channel drill bit with helix angles of 0° and 30° in two different orientations (front and side views). The intensity profiles are plotted along the highlighted reference lines on each figure. All MQL and camera settings were kept constant for all the experiments to minimize the uncertainty and extraneous errors from the setup. Moreover, the channel length was also kept the same for channels in both cases to ensure same interaction between the channel and the lubricant. The image processing method in the previous section was applied to all the cases to generate the projected flow distribution plots.

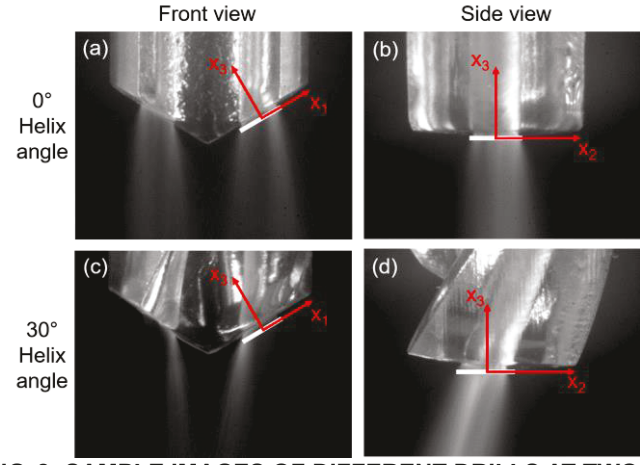
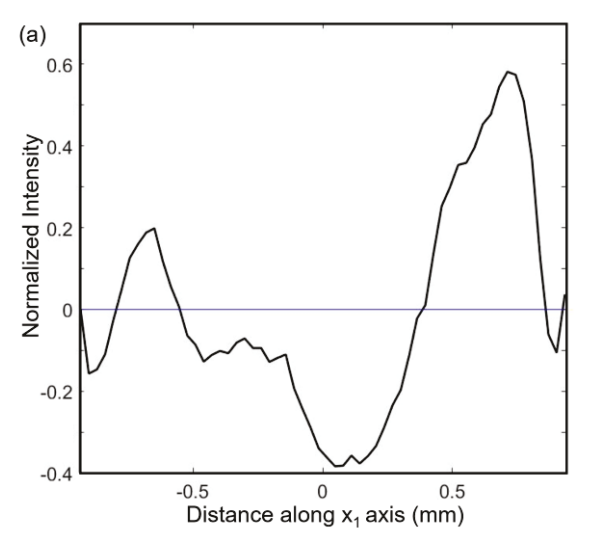
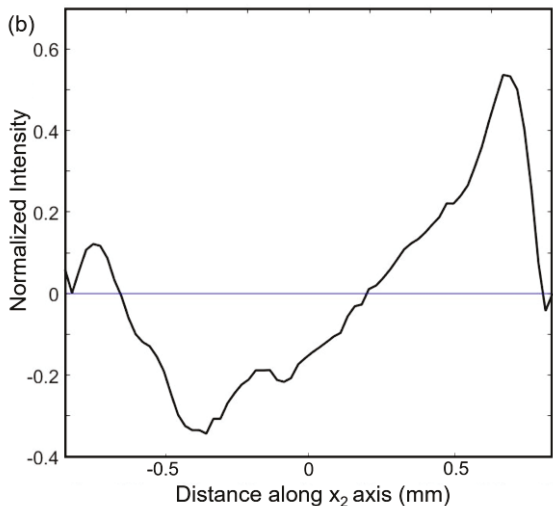


FIG. 8: SAMPLE IMAGES OF DIFFERENT DRILLS AT TWO ORIENTATIONS (THE WHITE LINE REPRESENT THE LINE ACROSS WHICH INTENSITY IS PLOTTED) (a) 0° HELIX ANGLE, FRONT VIEW (b) 0° HELIX ANGLE, SIDE VIEW (c) 30° HELIX ANGLE – SIDE VIEW

0° Helix Angle Channel

Figure 9(a) shows the projected flow structure in the front view and Fig. 9(b) shows the projected flow structure in the side view. The negative direction of the x1 axis points towards the axis of rotation of the drill and the negative x2 direction points towards the camera when looked from the front view. In the front view, the oil appears to concentrate toward two ends. The negative values at the ends are due to the expansion of the flow





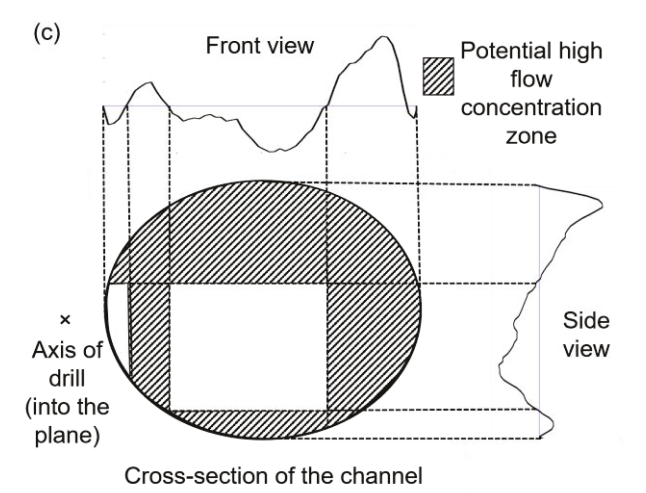
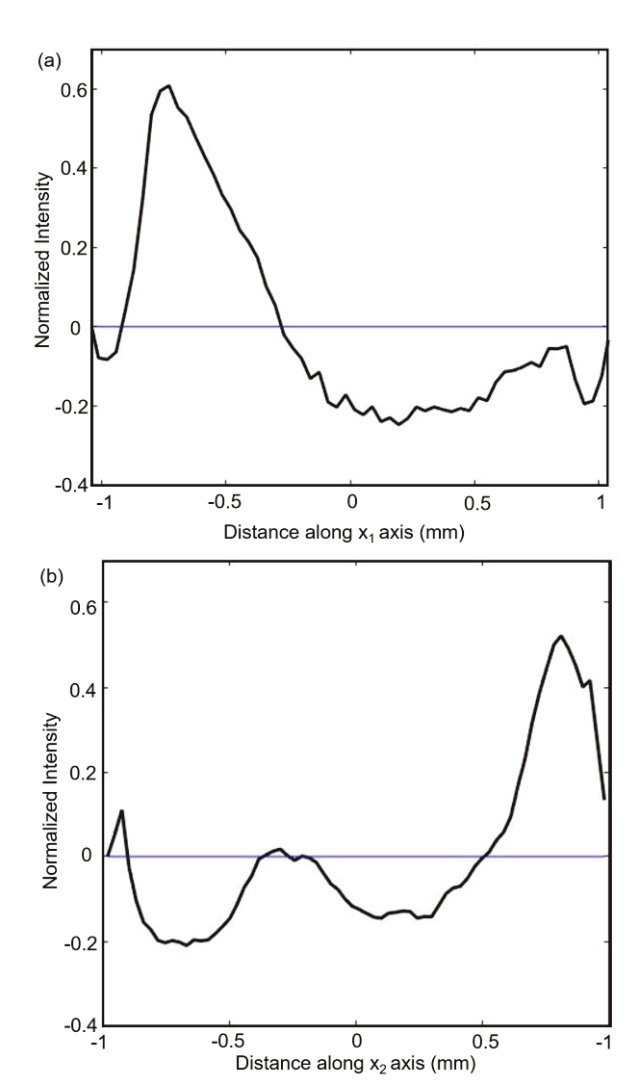


FIG. 9: (a) INTENSITY DIFFERENCE PROFILE 0 HELIX ANGLE FRONT VIEW (b) INTENSITY DIFFERENCE PROFILE 0° HELIX ANGLE SIDE VIEW (c) INTERPRETING THE PROFILES AND MAPPING THE OIL DISTRIBUTION ACROSS THE AREA

right after coming out of the channel. The side view has a similar trend where the mass flow rate increases towards the two ends. The profiles obtained for front and side views were used to map the potential areas of high oil concentration across the channel cross-section as shown in Fig. 9(c). Note that, this mapping does not specify the exact oil concentration zones; instead, it only tells that the oil droplets were concentrated at the periphery of the channel. The unshaded areas remain undetermined with only two views. The results obtained agree with the prediction provide by Weisman et al.[29], which proves that the experimental results are correct.

30° Helix angle channel

Figure 10(a) shows the projected flow structure in front view of the 30° helix angle and Fig. 10(b) shows the projected flow structure in side view. The major and minor axes of the elliptical cross-section of the channel no more remain aligned with the axes shown in Fig. 8(c) & (d). Because of the helix angle of the channel, the ellipse gets rotated by about 30 degree towards the camera as seen in Fig. 10(c). Different from the



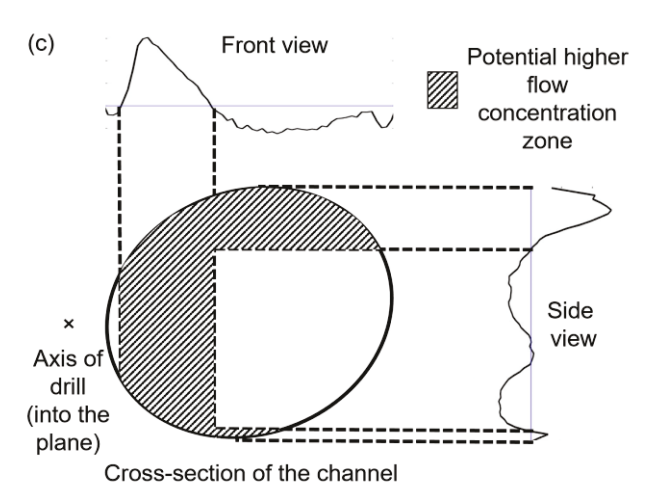


FIG. 10: (a) INTENSITY DIFFERENCE PROFILE 30° HELIX ANGLE FRONT VIEW (b) INTENSITY DIFFERENCE PROFILE 30° HELIX ANGLE SIDE VIEW (c) INTERPRETING THE PROFILES AND MAPPING THE OIL DISTRIBUTION ACROSS THE AREA

results of 0° helix angle, a noticeable higher oil flow rate was found towards the drill rotating axis (the negative x1-axis). Small negative values obtained in the proximity of start and end regions are due to flow expansion, as explained in the above section. For the side view, the oil distribution is mostly uniform except the back side of the drill bit (the positive x2-axis). The side view shows concentration of oil at the edges of the channel. When flow distribution was mapped across the channel cross-section (Fig. 10(c)), annular flow distribution with higher oil flow rate towards the chisel point of the drill can be seen. Again, the unshaded areas are undetermined.

COMPUTATIONAL FLUID DYNAMICS

A single phase CFD was conducted for the air flow since the majority of the two-phase flow (over 99%) in MQL was air. It is hypothesized that the mist flow distribution is highly dependent on the air flow field since the air flow carries the liquid droplets. This section details the construction of the CFD model for determining the flow field at the channel exit.

CFD Model Setup and Boundary Conditions

The CFD was solved using the FLUENT module on ANSYS for obtaining the velocity profile. Figure 11 shows the straight and helical channels used in the experiment. To reduce the computational effort, a finer mesh was applied near the channel wall which also helped to capture the boundary layer of the flow. Steady state flow of the air was assumed.

According to data provided by Ford Motor Company (Dearborn, MI), the average flow velocity inside the channel can be as high as 290 m/s for a 1-2 mm diameter channel for input pressure of 5.5 bar. The corresponding Reynolds number is over 30000, which means that the flow is highly turbulent. For this, the standard k- ϵ model was used. Researchers have developed a simplified single phase model for multiphase flow

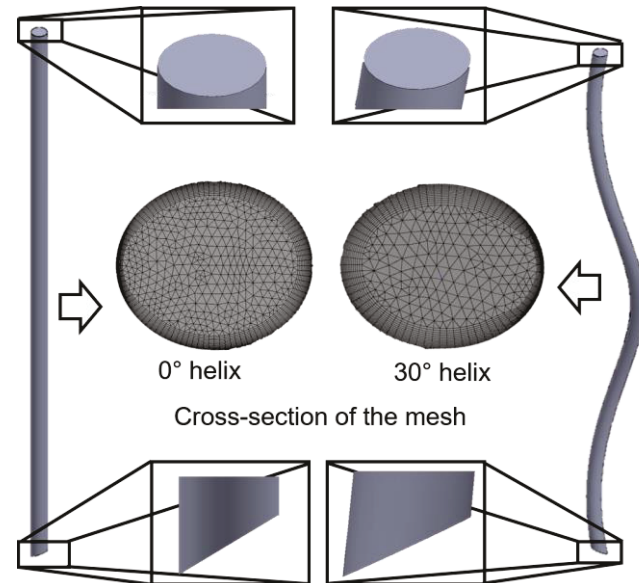


FIG. 11: MODELLED CONTROL VOLUME AND CROSS-SECTIONAL MESH

where, the density of the simulated fluid is the weighted average of the constituent fluids in multiphase flow. However, in the case of MQL, as stated earlier the volume fraction of oil is negligible as compared to air and thus, properties of air were directly used for simulation purposes. The Mach number at ambient conditions (300K) was calculated to be about 0.8, which is more than 0.3. Hence, compressibility effects need to be accounted for, because, the change in density of the fluid remains no longer negligible. Thus, a density based solver was used. Considering all the above facts, the boundary conditions used were inlet velocity as 290 m/s and exit pressure 1 atm. (zero gauge pressure at the exit). A no-slip boundary condition on the channel wall was assumed.

Simulation Results and Comparison

Figure 12 shows the velocity contours of the straight and helical channels, respectively, obtained at the exit cross-section of the channel as a result of CFD. In the straight channel (Fig. 12 (a)), the velocity was high in the core region of the channel which matches with velocity contours of a pipe flow. The flow field of the 30° helix angle channel (Fig. 12 (b)) shows the high velocity core shifting away from the axis of rotation of the drill. A significant slow velocity region was found toward the axis of the drill. This asymmetric velocity field occurs because of the centrifugal forces acting on the fluid when passing through the helical passage. The effect of the centrifugal force is documented in the literature as well [30]. The results obtained using CFD match with the results obtained in the literature [27, 30].

By comparing the velocity fields (Fig. 12) and flow distribution (Fig. 9(c) & 10(c)) in both the cases, it was obvious that the oil droplets concentrate in the low velocity zones. As discussed in the experimental results section, the oil concentration regions obtained in Fig. 9(c) and Fig. 10(c) does

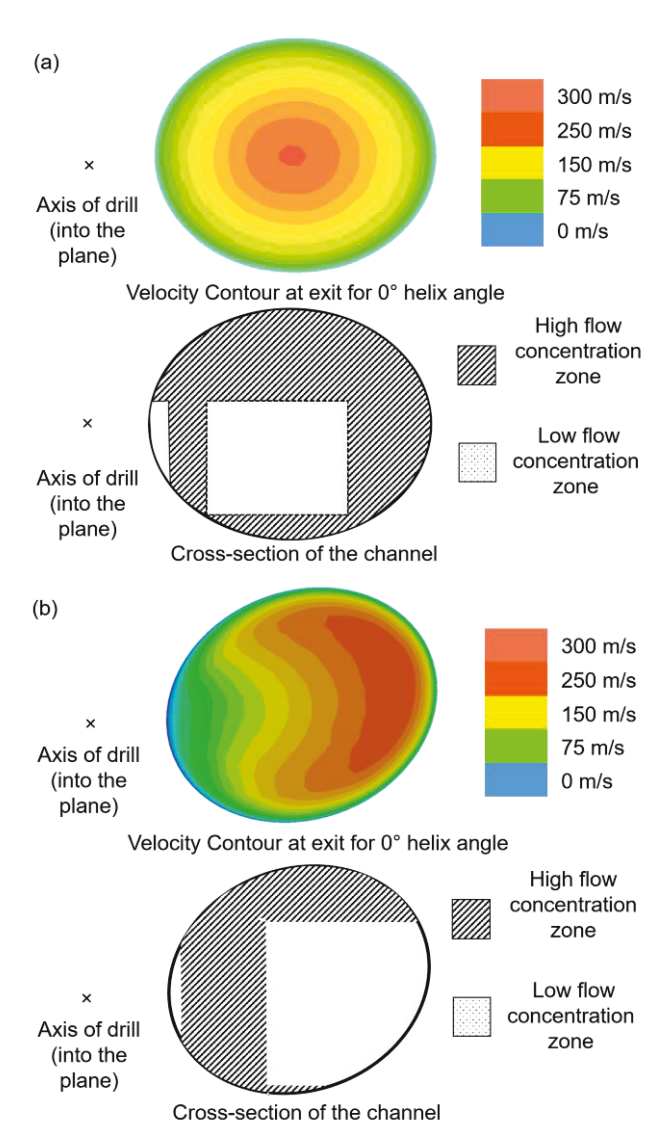


FIG. 12: CFD RESULTS AND COMPARISON WITH EXPERIMENTAL RESULTS (a) COMPARISON OF CFD AND EXPERIMENTAL RESULTS FOR 0° HELIX ANGLE CHANNEL (b) COMPARISON OF CFD AND EXPERIMENTAL RESULTS FOR 30° HELIX ANGLE CHANNEL

not mean that the areas highlighted are exact areas of high oil concentration. It becomes intuitive that, because of the projection of flow onto a plane, detailed mapping requires more views to confidently state the localized areas of high flow concentrations. Oil flow concentration in low velocity zones will be more evident if images from more angles are taken. In the 0° helix angle channel, a higher oil concentration was found towards the periphery of the channel where the air velocity was lower. In the 30° helix angle channel, a higher mass flow rate of the oil was found towards the drill chisel point i.e. the axis of the drill, where the air velocity was lower, along with small oil concentration zones at the periphery of the channel. According to simulation results for 30° helix angle channel, there is a low

velocity zone near the chisel tip of the tool, but the side view does not show oil concentration in that zone, one possible reason for that can be that the oil concentration at other locations along the view is so low that the high oil concentration at the tip gets compensated and the total intensity matches the baseline intensity. Nonetheless, based on the CFD results and experiments, there exists a strong correlation between the velocity contours and the mist flow distribution.

DISCUSSION

From the results, the oil droplets tend to gather in a low velocity region. This phenomenon can be explained by that the resistance to the flow is lower in a high velocity region, so the less viscous fluid tends to occupy the area with high velocity. This forces the more viscous fluid, such as oil droplets, to move towards the low velocity zones. In the 0° helix angle channel, oil is pushed towards the wall, because, the velocity was higher in the core region and lower in the outer region. For air being less viscous, it always tries to occupy the region with a higher velocity. For the 30° helix angle channel, since the flow field gets distorted due to the centrifugal force acting during flow through the helical passage, the oil flow distribution also changes accordingly to have more oil mass flow towards the center of the drill bit i.e. towards the chisel edge.

The current research was limited to a qualitative analysis of the oil flow distribution. However, the finding is important as, in the future, MQL flow can be predicted using simply a single phase flow CFD, which is more practical. For more quantitative analysis, the 3D flow distribution can be possibly reconstructed if multiple angles of views are taken and analyzed using the proposed image processing method.

Another limitation of this study is the naturally pulsed flow of MQL system. Despite a high frequency, the mist flow is not a completely continuous stream. Instead, the mass flow rate varies slightly over time. The normalization can diminish this effect only up to a certain extent. From the measurement perspective, it is important to synchronize the image acquisition with the flow pulse to ensure that the measurement is always taken at the same mass flow rate.

CONCLUSION AND FUTURE WORKS

The study presented a method to analyze the flow structure for MQL through-tool channel drill bit. This method was applied to compare two circular channels with 0° and 30° helix angles. The major finding is that the distribution of oil droplets in MQL mist flow is highly related to the velocity profile. This is confirmed by comparing the measured flow structure and CFD simulated velocity field. This means, a single phase CFD can be used to estimate the multiphase flow distribution without a time-consuming simulation such as Volume of Fluid (VOF) or SPH-CFD coupled analysis.

Based on the results, the helical angle can change the flow field and thus affect the oil distribution. Therefore, the shape and size of channels are also expected to change the oil droplet distribution in a flow. It can be concluded that channel geometry plays an important role in MQL flow distribution, which in turn determines the machining performance.

To advance the current study, the future work includes experimentation for different channel cross-sectional shapes and areas, incorporating the effect of surface roughness on the oil distribution, flow distribution during the cutting conditions. Furthermore, for detailed tomographic regeneration of the 3D profile image acquisition and processing will be carried out from multiple angles. Effect of the workpiece material, which creates a back pressure on the fluid delivery channel will also be worked on.

ACKNOWLEDGMENTS

The authors to would like to thank NSF (Grant #1760985), Dr. Stephenson from Ford Motor Company (Dearborn, MI) to provide the velocity data; Mr. Walker from UNIST Inc.(Grand Rapids, MI) for providing the MQL system. Also, thank you Behrouz Takabi and Yi-Tang Kao for their helpful inputs throughout the research.

REFERENCES

- [1] Bruni, C., Forcellese, A., Gabrielli, F., and Simoncini, M., 2006, "Effect of the lubrication-cooling technique, insert technology and machine bed material on the workpart surface finish and tool wear in finish turning of AISI 420B," International Journal of Machine Tools and Manufacture, 46(12), pp. 1547-1554.
- [2] Tai, B. L., Stephenson, D. A., and Shih, A. J., 2012, "An Inverse Heat Transfer Method for Determining Workpiece Temperature in Minimum Quantity Lubrication Deep Hole Drilling," Journal of Manufacturing Science and Engineering, 134(2), pp. 021006-021006-021008.
- [3] Chen, Z., Atmadi, A., Stephenson, D. A., Liang, S. Y., and Patri, K. V., 2000, "Analysis of Cutting Fluid Aerosol Generation for Environmentally Responsible Machining," CIRP Annals, 49(1), pp. 53-56.
- [4] Sutherland, J. W., Kulur, V. N., King, N. C., and von Turkovich, B. F., 2000, "An Experimental Investigation of Air Quality in Wet and Dry Turning," CIRP Annals, 49(1), pp. 61-64
- [5] Tai, B. L., Stephenson, D. A., Furness, R. J., and Shih, A. J., 2014, "Minimum Quantity Lubrication (MQL) in Automotive Powertrain Machining," Procedia CIRP, 14, pp. 523-528.
- [6] Heinemann, R., Hinduja, S., Barrow, G., and Petuelli, G., 2006, Effect of MQL on the tool life of small twist drills in deep-hole drilling.
- [7] Filipovic, A., and Stephenson, D. A., 2006, "Minimum Quantity Lubrication (MQL) applications in automotive power-train machining," Machining Science and Technology, 10(1), pp. 3-22.
- [8] Vivek, T. G., Vikas, T. P., Kuppan, P., Balan, A. S. S., and Oyyaravelu, R., 2016, "Experimental investigation of machining parameter under MQL milling of SS304," IOP

- Conference Series: Materials Science and Engineering, 149(1), p. 012023.
- [9] Tai, B. L., Jessop, A. J., Stephenson, D. A., and Shih, A. J., 2012, "Workpiece Thermal Distortion in Minimum Quantity Lubrication Deep Hole Drilling—Finite Element Modeling and Experimental Validation," Journal of Manufacturing Science and Engineering, 134(1), pp. 011008-011008-011009.
- [10] Lerma, I., Jimenez, M., Edinbarough, I., Krell, J., and Hung, N. P., 2015, "Characterization of Micromist for Effective Minimum Quantity Lubrication," Advanced Materials Research, 1115, pp. 43-46.
- [11] Le Coz, G., Marinescu, M., Devillez, A., Dudzinski, D., and Velnom, L. J. A. T. E., 2012, "Measuring temperature of rotating cutting tools: Application to MQL drilling and dry milling of aerospace alloys," 36, pp. 434-441.
- [12] Kuzu, A. T., Berenji, K. R., Ekim, B. C., and Bakkal, M., 2017, "The thermal modeling of deep-hole drilling process under MQL condition," Journal of Manufacturing Processes, 29, pp. 194-203.
- [13] Tawakoli, T., Hadad, M., and H. Sadeghi, M., 2010, Influence of oil mist parameters on minimum quantity lubrication MQL grinding process.
- [14] Davim, J., Sreejith, P. S., and Silva, J., 2007, Turning of Brasses Using Minimum Quantity of Lubricant (MQL) and Flooded Lubricant Conditions.
- [15] Attanasio, A., Gelfi, M., Giardini, C., and Remino, C., 2006, "Minimal quantity lubrication in turning: Effect on tool wear," Wear, 260(3), pp. 333-338.
- [16] Li, Q., Lerma, I., Alvarado, J., Edinbarough, I., and Hung, W. N. P., 2015, "Characterization of Micromist for Effective Machining," (57359), p. V02AT02A058.
- [17] Chen, M., Jiang, L., Shi, B. W., Liu, Z. Q., and An, Q. L., 2012, "CFD Analysis on the Flow Field of Minimum Quantity Lubrication during External Thread Turning," Materials Science Forum, 723, pp. 113-118.
- [18] Tasdelen, B., Wikblom, T., and Ekered, S., 2008, "Studies on minimum quantity lubrication (MQL) and air cooling at drilling," Journal of Materials Processing Technology, 200(1), pp. 339-346.
- [19] Sharma, A. K., Tiwari, A. K., and Dixit, A. R., 2016, "Effects of Minimum Quantity Lubrication (MQL) in machining processes using conventional and nanofluid based cutting fluids: A comprehensive review," Journal of Cleaner Production, 127, pp. 1-18.
- [20] Rahim, E. A., and Dorairaju, H., 2018, "Evaluation of mist flow characteristic and performance in Minimum Quantity Lubrication (MQL) machining," Measurement, 123, pp. 213-225.
- [21] Sovani, S. D., Chou, E., Sojka, P. E., Gore, J. P., Eckerle, W. A., and Crofts, J. D., 2001, "High pressure effervescent atomization: effect of ambient pressure on spray cone angle," Fuel, 80(3), pp. 427-435.
- [22] Husted, B. P., Petersson, P., Lund, I., and Holmstedt, G., 2009, "Comparison of PIV and PDA droplet velocity

- measurement techniques on two high-pressure water mist nozzles," Fire Safety Journal, 44(8), pp. 1030-1045.
- [23] Park, K.-H., Olortegui-Yume, J., Yoon, M.-C., Kwon, P. J. I. J. o. M. T., and Manufacture, 2010, "A study on droplets and their distribution for minimum quantity lubrication (MQL)," 50(9), pp. 824-833.
- [24] Powell, R. L., 2008, "Experimental techniques for multiphase flows," 20(4), p. 040605.
- [25] Maruda, R. W., Krolczyk, G. M., Feldshtein, E., Pusavec, F., Szydlowski, M., Legutko, S., and Sobczak-Kupiec, A., 2016, "A study on droplets sizes, their distribution and heat exchange for minimum quantity cooling lubrication (MQCL)," International Journal of Machine Tools and Manufacture, 100, pp. 81-92.
- [26] Tai, B. L., Dasch, J. M., and Shih, A. J., 2011, "Evaluation and comparison of lubricant properties in Minimum Quantity Lubrication machining," Machining Science and Technology, 15(4), pp. 376-391.
- [27] A. S, J., Hewson, R., Merson, E., Summers, J., and Thompson, H., 2014, Internal twist drill coolant channel modelling using Computational Fluid Dynamics.
- [28] Kao, Y.-T., Takabi, B., Hu, M., and Tai, B. L., 2017, "Coolant Channel and Flow Characteristics of MQL Drill Bits: Experimental and Numerical Analyses," (50732), p. V002T003A031.
- [29] Weisman, J., and Kang, S. Y., 1981, "Flow pattern transitions in vertical and upwardly inclined lines," International Journal of Multiphase Flow, 7(3), pp. 271-291.
- [30] Yamamoto, K., Alam, M. M., Yasuhara, J., and Aribowo, A., 2000, "Flow through a rotating helical pipe with circular cross-section," International Journal of Heat and Fluid Flow, 21(2), pp. 213-220.